RMetS
Royal Meteorological Society

Conditions under which CNOP sensitivity is valid for tropical cyclone adaptive observations

Xiaohao Qin,[a] Wansuo Duan[a]* and Mu Mu[b]

[a]*LASG, Institute of Atmospheric Physics, Chinese Academy of Sciences, Beijing, China*
[b]*Key Laboratory of Ocean Circulation and Wave, Institute of Oceanology, Chinese Academy of Sciences, Qingdao, China*

*Correspondence to: W. Duan, LASG, Institute of Atmospheric Physics, Chinese Academy of Sciences, Beijing 100029, China. E-mail: duanws@lasg.iap.ac.cn

To determine whether profound improvements in tropical cyclone (TC) forecasting are achievable by deploying dropwindsondes according to conditional nonlinear optimal perturbation (CNOP) sensitivity, observing system simulated experiments (OSSEs) were conducted on 20 TCs that developed over the western North Pacific during 2010 using Mesoscale Model 5 and its 3DVar assimilation system. Of the 20 cases, 13 showed neutral or improved track forecasts of between 0% and 51.2%. Eliminating initial errors within the CNOP pattern, which are related to either the storm directly or the surrounding regimes indirectly, reduced the subsequent track forecast errors. The remaining 7 TCs showed deterioration in the accuracy of the track forecasts over the 48 h forecast period. Accurate forecasts made without adaptive observations, a low sensitivity of forecast errors to initial errors, or major forecast errors associated with regimes other than the TC, can lead to a decline in the accuracy of TC track forecasts.

Following analysis of the potential causes of inaccuracy in the track forecasts, we find that TC cases with profound positive effects on track forecasts often satisfy the following four conditions: (i) an inaccurate initial forecast without additional observation data; (ii) proper sensitivity of the forecast errors to the initial errors; (iii) a large proportion of the forecast errors fall within the verification region; and (iv) the TC system is the dominant regime in the verification region at verification time. Seven TCs satisfied these four conditions, and showed a mean reduction of 28.75% in track forecast errors over periods of 12–48 h. This result suggests that the TC cases satisfying these four conditions often show profound improvements on track forecast by dropwindsondes guided by CNOP sensitivity.

Key Words: tropical cyclone; adaptive observations; conditional nonlinear optimal perturbations; conditions; profound track forecast improvements

Received 23 July 2012; Revised 19 November 2012; Accepted 20 December 2012; Published online in Wiley Online Library 20 May 2013

Citation: Qin X, Duan W, Mu M. 2013. Conditions under which CNOP sensitivity is valid for tropical cyclone adaptive observations. *Q. J. R. Meteorol. Soc.* **139**: 1544–1554. DOI:10.1002/qj.2109

1. Introduction

Many factors have contributed to recent improvements in tropical cyclone (TC) track forecasts, including the use of advanced numerical models, satellite observations, and adaptive observations obtained by dropwindsondes, aircrafts, balloons, ships, etc. (Aberson, 2002, 2003). Dropwindsondes are an important tool for the collection of adaptive observational data, and increasing numbers have been released in data-sparse TC environments and inner

cores since 1982 (Burpee *et al.*, 1996), yielding significant improvements in numerical track forecasts. Reductions of 10–15% in Global Forecast System (GFS) TC track forecast errors were achieved by the synoptic surveillance missions of TCs over the Atlantic (Aberson, 2010). In addition, the Dropwindsonde Observations for Typhoon Surveillance near the Taiwan Region (DOTSTAR) project began in the Pacific in 2003 (Wu *et al.*, 2005, 2007), and statistical results from DOTSTAR (2003–2009) show that assimilation of dropwindsonde data leads to improvements of 60% of the cases in 1- to 5-day track forecasts, and 10–20% reductions in mean track error, with at least a 90% confidence level (Chou *et al.*, 2011).

Previous studies have also confirmed the beneficial effects of adaptive observations on TC track forecasts (Elsberry and Harr, 2008; Harnisch and Weissmann, 2010; Weissmann *et al.*, 2010, 2012), and show that these benefits are dependent upon the correct identification of the most appropriate regions (sensitive regions) for each adaptive observation mission. Among the methods used to identify these sensitive regions, the singular vectors (SVs; Palmer *et al.*, 1998) and ensemble transform Kalman filter (ETKF; Bishop *et al.*, 2001) are widely used. The SV method accounts for the analysis error statistics of the routine observational network by identifying structures that linearly evolve into the leading eigenvectors of the forecast error covariance matrix associated with the routine observational network and the localized verification region (Ehrendorfer and Tribbia, 1997). The ETKF technique is used to quantitatively estimate the reduction of the forecast error variance of each distinct deployment of observational resources by constructing ensemble-based approximations to the prediction error covariance matrices associated with rankings of different possible deployments of observational resources. Both methods have advantages and limits. ETKF can quantitatively estimate the impacts of specific adaptive observational networks concerning the verification regions based on the prediction error statistics, but makes greater demands on the ensemble sample, while SVs emphasize the dynamics of initial errors, but assume their linear evolution, a factor that cannot be ignored in ETKF either.

However, the motion of the atmosphere and oceans is dominated by complicated nonlinear systems, especially as the observation period increases. Hence, based on the SV principles, Mu *et al.*(2003) and Mu and Zhang (2006) proposed the conditional nonlinear optimal perturbation (CNOP) approach. CNOP is the initial perturbation whose nonlinear evolution attains the maximum of the cost function, which is constructed according to the physical problems of interest with physical constraint conditions. Similar to SVs, CNOP has been used to identify sensitive regions in the forecast of heavy rain and typhoons (Mu *et al.*, 2009; Wang and Tan, 2009; Chen, 2011; Chen and Mu, 2012; Qin and Mu, 2011a, 2011b; Wang *et al.*, 2011; Zhou and Mu, 2011, 2012a, 2012b). Qin and Mu (2011b) used the observing system simulation experiments (OSSEs) to study the effects of CNOP and SV sensitivities on TC track forecasts. They found an improvement in forecast accuracy in six of seven cases, with the degree of improvement being between 13% and 46% in the CNOP-sensitive regions, and 14–25% in the leading five SV-sensitive regions, which demonstrates the effectiveness of CNOP sensitivity in reducing TC track forecast errors. These previous findings support the use of CNOPs in future research into the use of adaptive observations in TC forecasting.

Nevertheless, improvements in TC track forecasts based on adaptive observations have not been universal. Field experiments conducted in the Atlantic and Pacific oceans (Langland *et al.*, 1999) showed that the forecast accuracy in 20–30% of the cases studied was either unaffected or declined following the assimilation of the additional data. These findings are in line with the statistical results of DOTSTAR from 2003 to 2009; i.e. only minor improvements, or even deteriorations, occurred in nearly one third of the TC cases where dropwindsonde data were incorporated into the TC track forecasts (Chou *et al.*, 2011). That is to say, majority of the TC cases can benefit from adaptive observations, while the others cannot. Therefore, are there some common characteristics among those cases with profound track forecast improvements? This is the motivation for the present study.

This question is addressed by analyzing the impacts of CNOP sensitivity on the TC track forecasts of 20 cases that originated in the western North Pacific during the 2010 season, with the aim of providing a theoretical reference for future operational decisions regarding the appropriateness of adaptive observation missions. The remainder of this paper is organized as follows. Section 2 describes the CNOP adaptive observation methods used in this study and section 3 presents the strategy. Section 4 describes the TC events studied, and then considers the OSSE results and details the conditions required to lead to profound benefits from the use of adaptive observations based on CNOP sensitivity. Finally, the conclusions and discussion are presented in section 5.

2. Conditional nonlinear optimal perturbations

CNOPs, which represent the largest-growing perturbations in a nonlinear sense, have been used in the predictability of ENSO events (Duan *et al.*, 2004, 2009; Mu *et al.*, 2007; Yu *et al.*, 2009, 2012a, 2012b; Duan and Luo, 2010), the thermohaline circulation (Mu *et al.*, 2004; Sun *et al.*, 2005), blocking events (Jiang and Wang, 2010; Jiang *et al.*, 2011; Mu and Jiang, 2011), cold vortex (Jiang and Wang, 2011), and simulation and predictability of ecosystem (Sun and Mu, 2009, 2011, 2012; Sun *et al.*, 2010).

Consider a nonlinear model M acting on a state vector X, such that $X_t = M(X_0)$, where the subscript refers to the integration time. Let δX_0 and δX_t represent the initial and final perturbation states, respectively, such that $X_t + \delta X_t = M(X_0 + \delta X_0)$. For a chosen norm $||\cdot||$, an initial perturbation δX_0^* of δX_0 is called the CNOP if, and only if

$$J(\delta X_0^*) = \max_{||\delta \mathbf{X}_0|| \le \beta} ||M(X_0 + \delta X_0) - M(X_0)|| \qquad (1)$$

where $||\delta X_0|| \le \beta$ is the initial constraint defined by the chosen norm $||\cdot||$, which could reflect some physical laws that the initial perturbation should satisfy. The norm $||\cdot||$ also measures the evolution of the perturbations in this study.

CNOP is the initial perturbation whose nonlinear evolution attains the maximal value of the cost function J at time t (Mu *et al.*, 2003; Mu and Zhang, 2006). In predictability studies, CNOP represents the initial error

that has the worst effect on the prediction result at the optimization time (Mu *et al.*, 2003). Therefore, CNOP has been used to identify the initial error that causes the largest prediction error for TC events (Mu *et al.*, 2009). That is to say, the worst forecast would be avoided if the CNOP is eliminated in the initial analysis. For the MM5 model, the sensitivities of CNOP to verification and horizontal resolution were investigated by Zhou and Mu (2011, 2012a). Based on these studies, in this paper the initial errors that cause significant forecast errors are identified in an attempt to reveal the impacts on TC track forecast of CNOP sensitivity. A local projection operator was acting on the cost function to ensure that computation was restricted to the verification region.

To compute CNOP, Eq. (1) must be solved, which is a maximization optimization problem, but one for which there is no solver available to calculate it. However, there are many solvers available to tackle minimization optimization problems. Therefore, Eq. (1) is converted into a minimization problem by considering the negative of the cost function, after which solvers such as Spectral Projected Gradient 2 (SPG2; Birgin *et al.*, 2001), Sequential Quadratic Programming (SQP; Powell, 1982), and Limited memory Broyden–Fletcher–Goldfarb–Shanno (L-BFGS; Liu and Nocedal, 1989) etc., can be used to compute the CNOP. In these solvers, the gradient of the modified cost function is required, and the adjoint of the corresponding model is usually used to obtain this gradient. Having calculated the gradient, running these solvers with initial guesses can find the minimum of the modified cost function (i.e. the maximum of the cost function in Eq. (1)) along the descendent direction of the gradient. In phase space, the point corresponding to the minimum of the modified cost function is the CNOP defined by Eq. (1). In this paper, the SPG2 solvers were used to obtain the CNOP of the MM5 model. If several initial guesses exist that converge to a point in the phase space, this point can be considered as a minimum in a neighbourhood. Thus several such points are obtained. Of these points, the one that makes the cost function in Eq. (1) the largest is regarded as the CNOP.

3. Strategy

The CNOP employed in this study optimized the perturbation energy growth over a 48 h optimization period using adjoint models of MM5. The physical parametrizations used in the simulation include the dry convective adjustment, grid-resolved large-scale precipitation, the high-resolution PBL scheme, and the Kuo cumulus parametrization scheme. The horizontal area covered a 121×81 square lattice with a horizontal resolution of 60 km, and 11 vertical levels, with the top level at 50 hPa. The verification region was approximately a $15^\circ \times 12^\circ$ box centred on the forecast central position of the corresponding TC at 48 h.

In this paper, the total dry energy norm was used to measure the initial perturbations and their evolution, which can be expressed as follows:

$$G_{de}(\delta X_0) = \frac{1}{D}\int_D \int_0^1 [u'^2_0 + v'^2_0 + \frac{c_p}{T_r} T'^2_0 + R_a T_r \left(\frac{p'_s}{p_r}\right)^2] \mathrm{d}\sigma \mathrm{d}s \quad (2)$$

where D is the horizontal model region, σ is the vertical coordinate, $c_p = 1005.7$ J kg^{-1} K^{-1}, which is the specific heat at constant pressure, $R_a = 287.04$ J kg^{-1} K^{-1}, which is the dry air constant, $p_r = 1000$ hPa, and $T_r = 270$ K. δX_0 is composed of u'_0, v'_0, T'_0, and p'_s, which are the perturbed zonal and meridional wind components, temperature, and surface pressure, respectively. The integration extends over the full domain D and the vertical direction σ. In this study, specific humidity was not considered in the cost function or in the initial perturbation, but the moisture equation was included in the model. According to Eq. (2), CNOP sensitivity comprises those grids with higher perturbation energy.

After identifying the CNOP sensitivity, OSSEs were completed in these regions for each individual case to estimate the impacts of CNOP sensitivity on TC track forecasts. Generally, three basic components should be included in OSSEs (Hoffman *et al.*, 1990): a 4D reference atmosphere, often called the nature run, the purpose of which is to act as the 'truth', a procedure to obtain simulated observations by sampling the nature run and adding errors, and a data assimilation system, which comprises a forecast model and the analysis procedure.

In this study, the truth was taken to be forecasts from 0 to 48 h based on National Centers for Environmental Prediction (NCEP) reanalysis data, using the MM5 model and the same resolution and physical parameterizations as those used for calculating the CNOP aforementioned. The forecast TC centres were collated every 6 h to represent the true TC tracks. In order to estimate the statistics of the OSSE truth run to reality, we compare the simulated TC centres in OSSE truth run with the best track from the Joint Typhoon Warning Center (JTWC). We find that the difference increases monotonically as the forecast period increases, being 92.4 km at 12 h to 325.9 km at 48 h averagely for all 20 cases. The simulation within 24 h of the OSSE truth run has comparative track forecast errors with those in National Hurricane Center (NHC) for Atlantic basin tropical storms and hurricanes from 2000 to 2009. However, the track forecast errors of the OSSE truth run over 30 h are larger, but not too much larger, than those in NHC from 2000 to 2009. Generally, the track forecast errors of the OSSE truth run in this study are acceptable. Forecasts during the same period with same model and resolution, using the ERA-Interim reanalysis data from the European Centre for Medium-Range Weather Forecasts (ECMWF), were used as the control run. The difference between the position of the TC centre in the control run and the nature run was defined as the error in the TC track forecast made without additional dropwindsonde data, which only come from using different initial reanalysis data.

After identifying the CNOP-sensitive regions for the optimization period (0–48 h), 15 simulated dropwindsondes were deployed at 0 h over these regions to obtain observational data, which were the sum of the reanalyses (interpolated to observational points) of the nature run at 0 h and randomly produced observation errors of the order of 10^{-1} of the analysis. The number of the dropwindsondes is decided by both the range of the sensitive region and the distance between two neighbour sondes. The simulated additional dropwindsonde data included horizontal wind speed, horizontal wind direction, and temperature at 850, 500, and 200 hPa. The 3DVar assimilation system of MM5 was used to assimilate the additional dropwindsonde data

to produce an analysis at 0 h, which was then run to predict the locations of the TC centres over the following 48 h. The difference between these TC centre positions and the nature run was defined as the TC track forecast error with dropwindsondes. The difference between these errors, and those without dropwindsondes, was used to evaluate the influence of CNOP sensitivity on TC track forecasts.

4. Results

4.1. TC cases

According to the China Meteorological Administration (CMA), 14 TCs originated in the western North Pacific during the 2010 season. Of these, Namtheum (No. 201008) lasted for less than 48 h, which was too short for the analytical approach used here, and this TC was not included in the study. During the period between 0000 UTC 29 August to 0000 UTC 2 September, three TCs developed simultaneously over the western North Pacific: Lionrock (No. 201006), Kompasu (No. 201007), and Namtheum (No. 201008). The control run could not simulate the spiral structure of Kompasu, leading to the exclusion of this event from the study. A similar simulation problem occurred with Mindulle (No. 201005), which was also excluded. If the lifetime of a TC was longer than 96 h, it will be separated into two continuous cases. Therefore, there are 20 cases (listed in Table 1) for the 11 TC events.

4.2. CNOP sensitivity and simulated dropping sites

For all 20 cases, the analysis at 0 h in the control run was used as the basic state from which to calculate CNOPs concerning the verification region (small rectangle in Figure 1) over the following 48 h optimization period. For example, consider the case of CHABA2, where the shaded areas (J kg^{-1}) in Figure 1 represent the sensitive regions identified by CNOP according to Eq. (2). Within this region, 15 simulated dropping sites were identified based on the restriction that the distance between adjacent sites was appropriate (about 150 km). Comparable figures for the other TCs have been omitted.

4.3. OSSE results

The simulated observational data were assimilated from the CNOP-sensitive regions for each TC case, and the track forecast errors were compared with and without dropwindsonde data at intervals of 6 h between 12 and 48 h. The average impact of dropwindsondes on the TC track forecast for each case is listed in the last column in Table 1, with negative values indicating an improvement. Neutral or improved track forecasts of between 0% and 51.2% were obtained from 13 of the TC cases (bold in Table 1). Of these 13 cases, 9 demonstrated a profound improvement (>10%), while the other 4 showed neutral or minor effects of between 0 and 4.6%. In contrast, deteriorations in forecast accuracy of between 7.8% and 72.5% occurred in 7 cases, with an average of 25.3%, which is a little less than the average profound improvement (26.3%). This result is in line with the findings of Chou *et al.*(2011).

Figure 2 shows the TC track forecast errors, with and without dropwindsonde data, every 6 h from 12 to 48 h, for each individual case. The points that plot beneath the diagonal line indicate that the track forecast errors with dropwindsondes are lower than those without dropwindsondes. The solid line in each colour represents the linear best fit of each set of data points of the same colour. Their slopes indicate the ratio of the track forecast errors with dropwindsondes to those without dropwindsondes. The shallower the slope, the larger the magnitude of improvement; conversely, if the slope is steeper than that of the diagonal, the use of sonde data results, on average, in a deterioration of the TC track forecast.

Figure 2(a) displays the results of the cases that showed profound improvements from the dropwindsondes deployed in CNOP-sensitive regions. Track forecast errors without dropwindsondes are evenly distributed between 0 and 400 km, suggesting that inaccurate forecasts were made without the adaptive observations. After assimilating the dropwindsonde data, most of the track forecast errors were reduced, which is highlighted by the concentration of data points in the lower right of the plot. Eight linear best-fit lines have shallower slopes than the diagonal line, indicating large-magnitude improvements in these cases. Compared with the cases with profound improvements, Figure 2(c) shows a totally different situation associated with the TCs for which the forecast became less accurate. Most of the points are grouped to the lower left corner of the plot, suggesting comparatively small track forecast errors made without the additional dropwindsonde data. Additionally, most of the points are above the diagonal line, which, together with the steeper slopes of the linear best-fit lines, confirms that the adaptive observations produced a less accurate forecast in these cases. The plot of the other four cases with neutral or minor improvements (Figure 2(b)) displays a transition between the previous two situations. Track forecast errors without dropwindsondes are typically less than 300 km, and the linear best-fit lines have a similar slope to the diagonal line. Neither indicates a pronounced degree of improvement.

As two examples of cases with profound improvements, detail for CHABA2 and Lionrock1 (Figure 3(a), (b)) shows that track forecast errors were reduced on average by 41.8% and 23.1%, respectively, after assimilating dropwindsonde data from CNOP-sensitive regions. For CHABA2, the CNOP sensitivity was along the forecast track between 0000 UTC 27 October and 0000 UTC 29 October in the control run (Figure 3(a1)). The forecast errors at 48 h are shown in Figure 3(a2). It is clear that the order of the energy at 48 h was much larger than that at 0 h, with an increase of approximately 638 times. This indicates that the forecast errors were sensitive to the initial error in this case. Therefore, if the order of initial errors is small, there would be a comparatively large order of forecast errors in the model region over a 48 h period. Moreover, most of the forecast errors were concentrated in the verification region, accounting for 51.68% of the error over the entire model region. This indicates that the forecast errors caused by CNOP were mainly within the verification region, and associated with the TC regime (concentrated around the TC central position at terminal time). That is to say, eliminating the initial errors associated with the CNOP pattern can directly reduce the forecast errors associated with the TC regime, rather than with other systems within the verification region.

The results from Lionrock1 were somewhat different from those from CHABA2. During the 48 h forecast

Table 1. 11 TCs originated in the western North Pacific during the 2010 season numbered (second column) according to the China Meteorological Administration (CMA).

Case	No.	Initial time	Terminal time	Impacts
OMAIS	201001	2010032406	2010032606	−51.20%
CONSON1	201002	2010071218	2010071418	21%
CONSON2		2010071418	2010071618	−1.48%
Chanthu	201003	2010072006	2010072206	7.77%
Dianmu	201004	2010080812	2010081012	9.49%
Lionrock1	201006	2010082900	2010083100	−23.11%
Lionrock2		2010083100	2010090200	−12.16%
Malou1	201009	2010090306	2010090506	13.27%
Malou2		2010090506	2010090706	15.60%
Meranti	201010	2010090800	2010091000	−22.66%
Fanapi1	201011	2010091606	2010091806	−16.46%
Fanapi2		2010091806	2010092006	0
Malakas1	201012	2010092106	2010092306	−0.45%
Malakas2		2010092306	2010092506	−4.63%
MEGI1	201013	2010101500	2010101700	72.52% %%
MEGI2		2010101700	2010101900	−13.59%
MEGI3		2010101900	2010102100	−20.14%
MEGI4		2010102100	2010102300	36.99%
CHABA1	201014	2010102500	2010102700	−35.45%
CHABA2		2010102700	2010102900	−41.77%

48 h optimization period from initial time ('2010032406' means 0600 UTC 24 March 2010, same below) up to terminal time for each case is shown in the third and forth columns, respectively. If the lifetime of a TC was longer than 96 h, it was separated into two continuous cases (as CONSON1 and CONSON2). The average impacts of dropwindsonde data in CNOP sensitivity on TC track forecast is displayed in the last column, with negative values indicating track forecast reduction. The corresponding TC cases with neutral or track forecast improvement are in bold type.

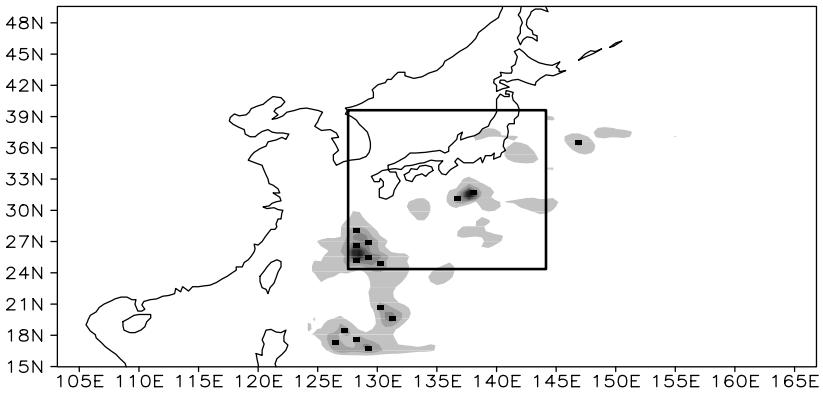

Figure 1. Sensitive regions (shaded; J kg^{-1}) calculated by CNOP in the small rectangle over 48 h optimization period for case CHABA2; squares represent the simulated sites for dropping sondes.

period, Lionrock1 remained a tropical depression, and was a comparatively weak system in the background. It was noticeable that the sensitive regions did not surround the TC centre position at 0 h, which was near Taiwan Island. The corresponding forecast errors at the end of the 48 h period (Figure 3(b2)) showed an increase of about 417 times compared with the initial errors, and were distributed into three parts, only 34.31% of which fell within the verification region. The western section was west of 100°E, the middle section was between 100°E and 115°E, and the eastern area was around Shanghai. These three areas of perturbation energy corresponded to different regimes. The centre of the South Asia high (located at 200 hPa) was over the western section (Figure 4(b)), which was the largest and most stable circulation regime during the northern summer. The situation in the middle section was more complicated. At the upper level, the easterly extension of the South Asia high controlled this region (Figure 4(b)), while at lower levels two different regimes contended with each other: a small, local anticyclone in the north, and a ridge over the South Asia continent (Figure 4(a)). Due to the topographic impact of Taiwan Island, a local cyclone formed near Shanghai. The main forecast errors were associated with these regimes rather than Lionrock1, and the subsequent development of Lionrock1 was, inevitably, jointly affected by the above regimes. The South Asia high controlled the upper level and western section, preventing the storm developing into a deep system, while the steering flow from both the system ahead of the ridge over South Asia, and the local anticyclone to the north, together pushed the storm east, where its progress was restricted within a small area near Taiwan Island. Hence eliminating initial errors with the CNOP pattern reduced forecast errors associated with the other systems, the steering flow of which in turn led to a more accurate track prediction of Lionrock1. This suggests that in this case the improved forecast accuracy was not due to the direct reduction of forecast errors associated with the storm itself, but to a

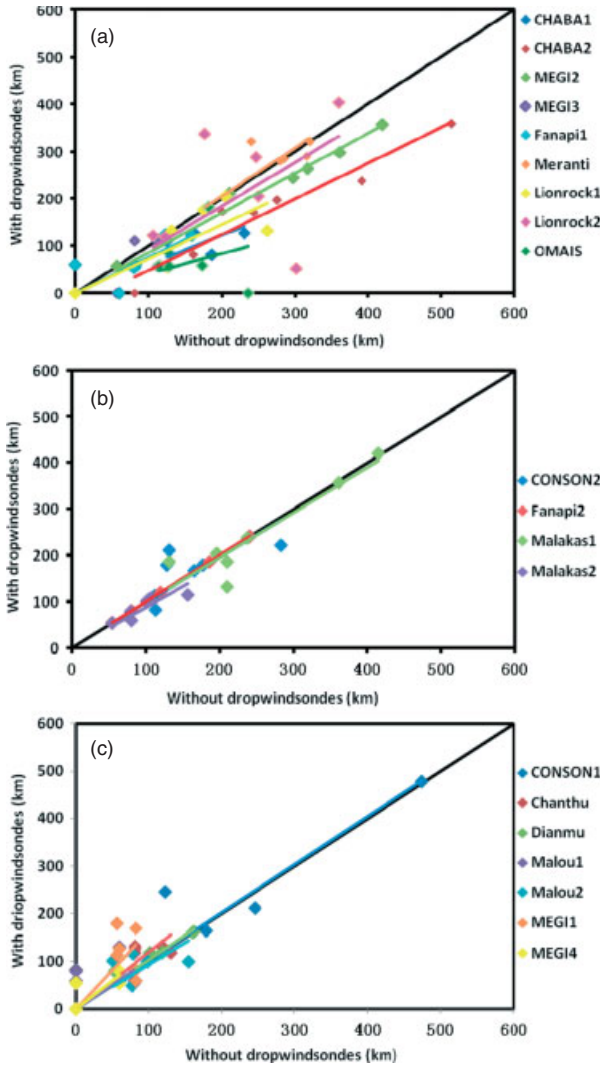

Figure 2. Scatter-plots of track forecast errors for each TC. The *y*-axis represents the errors associated with the track forecast made using additional dropwindsonde data, and the *x*-axis represents those made with no additional data. (a), (b), and (c) show those cases with profound improvements (above 10%), neutral or minor improvements, and a decline in the forecast accuracy, respectively.

more accurate estimation of the environmental systems that steered the subsequent movement of the TC.

Malakas1 was representative of a neutral impact on track forecast accuracy (see Figure 3(c3)), and developed from a tropical depression to a severe tropical storm. Most of the initial errors associated with the CNOP pattern (Figure 3(c1)) were located southwest of the storm with respect to its direction of movement. According to the streamlines at 500 hPa (Figure 4d) at 0 h, Malakas1 was southwest of the saddle between two subtropical highs (one over the central Pacific, the other over the western Pacific), and the regions with large initial errors corresponded to an inflow south of the storm from lower (925 hPa, Figure 4(c)) to mid levels (500 hPa, Figure 4(d)). This suggests that the initial errors related to the inflow from these areas would lead to the most forecast errors within the verification region. Over the following 48 h period, the errors increased 125 times to those at the initial time, which was comparatively smaller than in the previous two cases. With a comparable order of initial errors, the development of forecast errors for Malakas1 did not reach the magnitude of the other two cases. This indicates that the forecast errors were not so dependent on the initial errors in this case, suggesting that other factors (such as model errors) were probably primarily responsible for the forecast errors. This may explain why assimilating additional observational data resulted in a nearly neutral impact on track forecast accuracy in this case, even though about 71.82% of the forecast errors were concentrated in the verification region and were associated with the storm regime.

These results illustrate that the reasons for improvements in forecast accuracy in each case were different, even though 13 of the 20 cases showed a neutral or improvement of between 0% and 51.2% from the deployment of sondes in the CNOP sensitive regions. Directly reducing initial errors associated with the case itself can lead to a more accurate forecast of the TC track, such as in the case of CHABA2, while reducing initial errors associated with nearby regimes around a TC may generate useful data regarding the steering flow, which can further improve the forecast of the subsequent movement of the storm, such as for Lionrock1. Except for cases with profound improvements, neutral or minor improvements were shown by four cases; e.g., for Malakas1, the initial errors were not the principal factor responsible for forecast errors at terminal time, suggesting that model errors, or other factors, should be improved in an attempt to generate a more accurate forecast.

Similarly, MEGI1 was selected as an example of a case in which there was a decline in forecast accuracy. This storm developed into a typhoon from a tropical storm over the 48 h period, and showed the largest decrease in forecast accuracy, with an average increase in track forecast errors of 72.52% (Figure 3(d3)). The track forecast error without dropwindsonde data, averaged over 48 h, was nearly 60 km, which might reasonably be considered to be a near perfect prediction. After assimilation of the sonde data, track forecast errors approximately doubled (104 km) as before. Initial errors with respect to the CNOP pattern are shown in Figure 3(d1). The main areas of perturbation energy were located south of 5°N. Meanwhile, there was a cyclone over the South Asia continent (not shown), uncertainty regarding which led to large forecast errors there over the 48 h period (Figure 3(d2)). Other forecast errors were concentrated in South China, which was also outside of the verification region. In addition, compared with the initial errors, forecast errors at the terminal time increased by only 9 times, indicating that initial errors did not lead to considerable forecast errors in this case. It is inferred that model errors, or some other reasons, caused the larger forecast errors, or that the simulation was robust, and large forecast errors could not occur in this case.

Examining all 7 cases that experienced a decline in forecast accuracy suggests a number of possible causes for this, including the sensitivity of forecast errors to system errors rather than initial errors, TC regimes being too weak to be dominant in the verification region, other strong regimes outside the verification region dominated the main forecast errors, or very accurate track forecasts made before the assimilation of the dropwindsonde data.

4.4. *Conditions leading to improvements*

Having estimated the impact of CNOP sensitivity on TC track forecasts, further analysis was performed on those TCs where the accuracy of the forecast either improved or

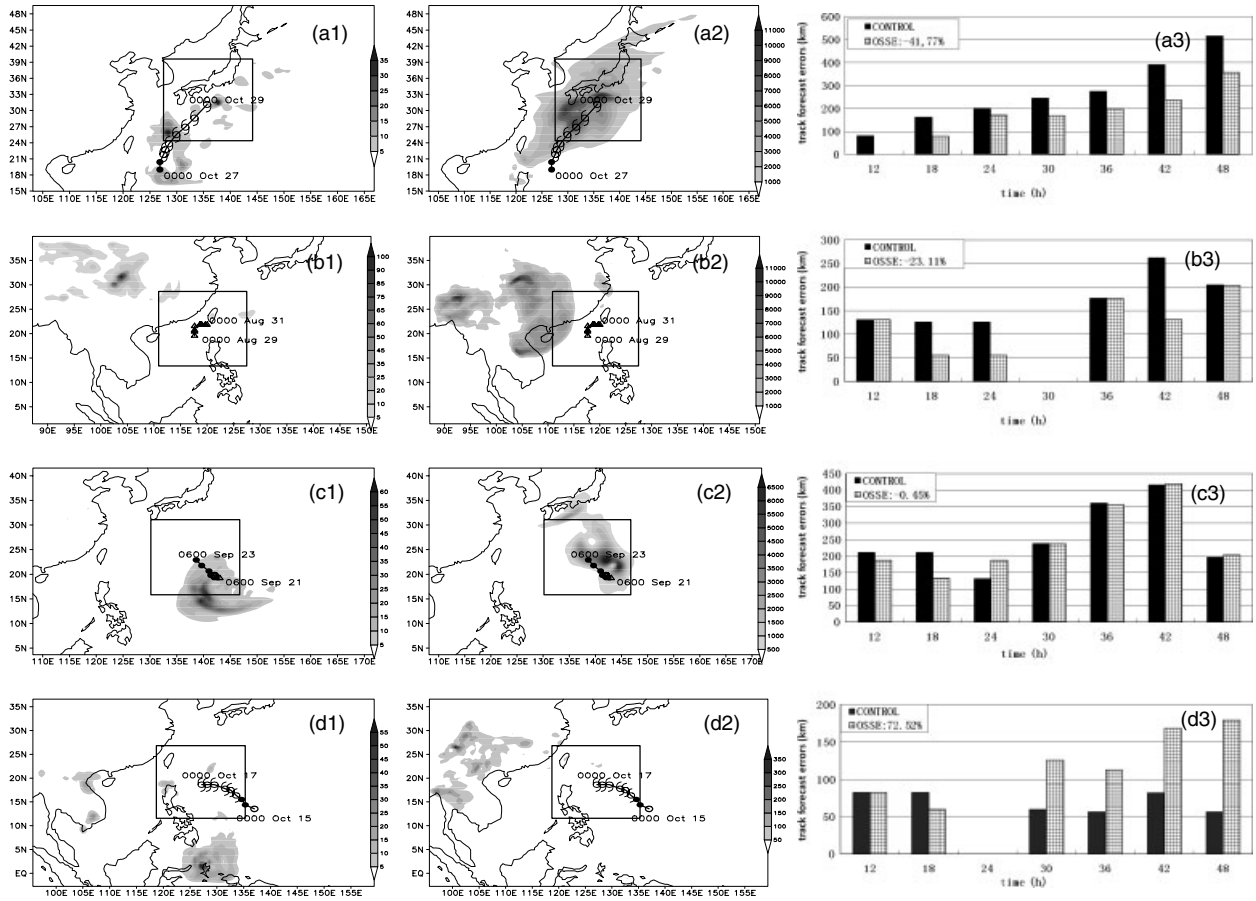

Figure 3. (1) CNOP sensitivity (shaded; J kg^{-1}), (2) corresponding forecast errors (shaded; J kg^{-1}) at terminal time (48 h), and (3) track forecast errors (km) from 12 to 48 h for TCs (a) CHABA2, (b) Lionrock1, (c) Malakas1, and (d) MEGI1.

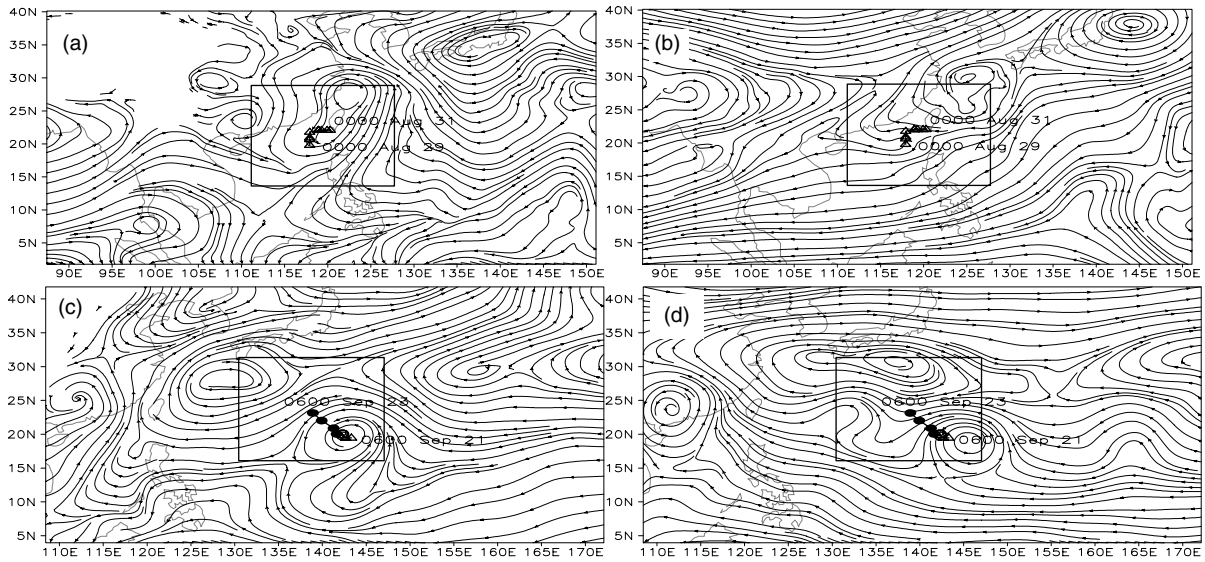

Figure 4. Streamlines at terminal time (48 h) at (a) 850 hPa and (b) 200 hPa for Lionrock1, and at initial time (0 h) at (c) 925 hPa and (d) 500 hPa for Malakas1.

declined. It was found that the TC cases where the track forecast errors could be reduced profoundly by dropping sondes according to CNOP sensitivity often satisfy following four conditions:

(i) The errors associated with the track forecast made without additional dropwindsonde data were not too small to distinguish.

(ii) The track forecast errors were properly sensitive to the initial errors.

(iii) The forecast errors in the verification region account for a large proportion of the errors across the whole model region.

(iv) The TC is the main atmospheric regime within the verification region.

These four points will be considered in more detail below.

With respect to the first condition, it is well known that adaptive observations are unnecessary for accurate forecasts. Generally, the average track forecast errors should be larger than the horizontal resolution. Otherwise, improvements are not obvious even if positive effects are obtained from the adaptive observations. However, under operational conditions, it is not possible to determine the track forecast errors without dropwindsonde data before the real observational data are obtained. In this case, track forecast differences between several predictions based on different models or different initial analyses can be used as an alternative reference.

The second condition emphasizes the importance of initial errors to adaptive observations, the principle of which is to improve the initial analysis by collecting additional observations. The evolution of these initial errors over a period should be obvious for a given constraint of initial errors (βin Eq. (1)). Taking CHABA2 as an example, the forecast errors at terminal time due to initial errors within the CNOP pattern increased approximately 638 times compared with those at the initial time. Conversely, the increase was only 9 times for MEGI1. That is to say, given initial errors with the same values, the initial errors caused much greater forecast errors for CHABA2 than for MEGI1, assuming that the model was perfect. This indicates that the forecast errors were much more sensitive in the former than the latter. Nevertheless, forecast errors cannot be too sensitive to initial errors. In this case (such as Malakas2), assimilation of dropwindsonde data with observational errors would cause only a small difference in initial analysis, which would in turn lead to very large forecast errors at terminal time.

The third condition guarantees that forecast errors are concentrated in the regions of interest. Only under this premise can adaptive observations reduce forecast errors within the verification region. Dianmu and MEGI1 are two cases in which this condition was not met, as forecast errors caused by initial errors of the CNOP pattern in the verification region only occupied 5.35% and 10.05%, respectively, of the total errors over the whole model region. Hence the areas affected mostly by the CNOP pattern's initial errors were outside the verification region. TC track errors would increase by 9.49% and 72.52%, respectively, for these two storms if the corresponding initial errors were eliminated.

The fourth condition must be more strictly applied than the third. Even if the forecast errors in the verification region account for a large proportion of the total errors across the model region, it is possible that the main forecast errors are caused by regimes other than the TC. Taking Fanapi2 as an example, over the 48 h period the forecast errors increased nearly 429 times from those at the initial time, and the forecast errors in the verification region accounted for 42.32% of the total errors. However, a local atmospheric regime but not the storm dominated the forecast errors. Hence dropwindsonde data did not help to reduce the track forecast errors associated with the TC, or no deterioration either.

It should be noted that the steering flow plays an important role in controlling the movement of TCs. Hence reducing the forecast errors associated with the surrounding atmospheric conditions can improve the TC forecast accuracy to some degree. Lionrock1 and Lionrock2 provided examples of this situation. However, the above criterion is not against the experience actually. Moreover, as a necessary condition that TC with profoundly improvements by dropping sondes often satisfies, it is indispensable.

Based upon these four conditions, the 20 TC cases were divided into three groups (Figure 5). The first comprises the 7 cases that satisfied all four conditions; the other two groups contain the rest. The difference between these latter two groups is that 6 cases showed neutral or improvements in track forecast after utilizing dropwindsonde data, while the other 7 showed deterioration. Taking OMAIS (Figure 5(a)) as an example, the shaded areas indicate the forecast errors caused by the CNOP pattern's initial errors at terminal time, from which it is possible to judge whether the TC regime dominated the forecast errors in the verification region. The three numbers in the upper left corner of the plot refer to the first three conditions: 153.71 is the mean (from 12 up to 48 h) track forecast error (km) without dropwindsonde data, forecast errors at terminal time increased 144.17 times over the 48 h period, and about 62.71% of these errors were concentrated in the verification region. Bold numbers indicate that the corresponding condition was not satisfied. Hence all four conditions can be reflected in one plot.

For the 7 cases that satisfied all four conditions, it is clear that the majority of the forecast errors at terminal time was concentrated in the verification region, and was associated with the TC regimes (Figure 5(a–g)). On average, the mean track forecast error from 12 to 48 h was 177 km in these cases, forecast errors increased 458 times compared with the initial errors within the CNOP pattern, and 51.8% of the forecast errors were concentrated in the verification region. Based upon these conditions, a mean 28.75% reduction in track forecast errors was obtained after assimilating dropwindsonde data according to CNOP sensitivity. This suggests that the TC track forecasts are likely to benefit from adaptive observations based on CNOP sensitivity if they satisfy the above four conditions.

For the 6 cases that did not satisfy all four conditions, but still showed neutral or some improvements in forecast accuracy, the forecast errors of four of the TCs was not associated with the TC regime (Figure 5(h–k)), while Malakas1 and 2 showed different sensitivities of forecast errors to initial errors: one is not so sensitive (Figure 5(l)); the other is too sensitive (Figure 5(m)). Generally, these 6 cases satisfy three of the four conditions. However, the situation for the cases in which the forecast accuracy fell is different. A common characteristic is the concentration of forecast errors outside of the verification area, which breaks the third condition (i.e. that the majority of the forecast errors should be associated with the TC regime). In addition, for three TCs (Figure 5(q), (s), (t)) the original track forecasts (without the adaptive sonde data) were exceptionally accurate, and this prevented any further improvements in these cases.

5. Conclusion and discussion

To determine the conditions under which profound improvements in TC track forecasts can be obtained by deploying dropwindsondes according to CNOP sensitivity, OSSEs were performed on 20 TC cases that originated in the western North Pacific during 2010 to measure the impact of CNOP sensitivity on track forecast accuracy. Based on these results, further analysis was conducted to determine the characteristics of the TC cases that showed profound improvements in track forecast accuracy. Finally, four

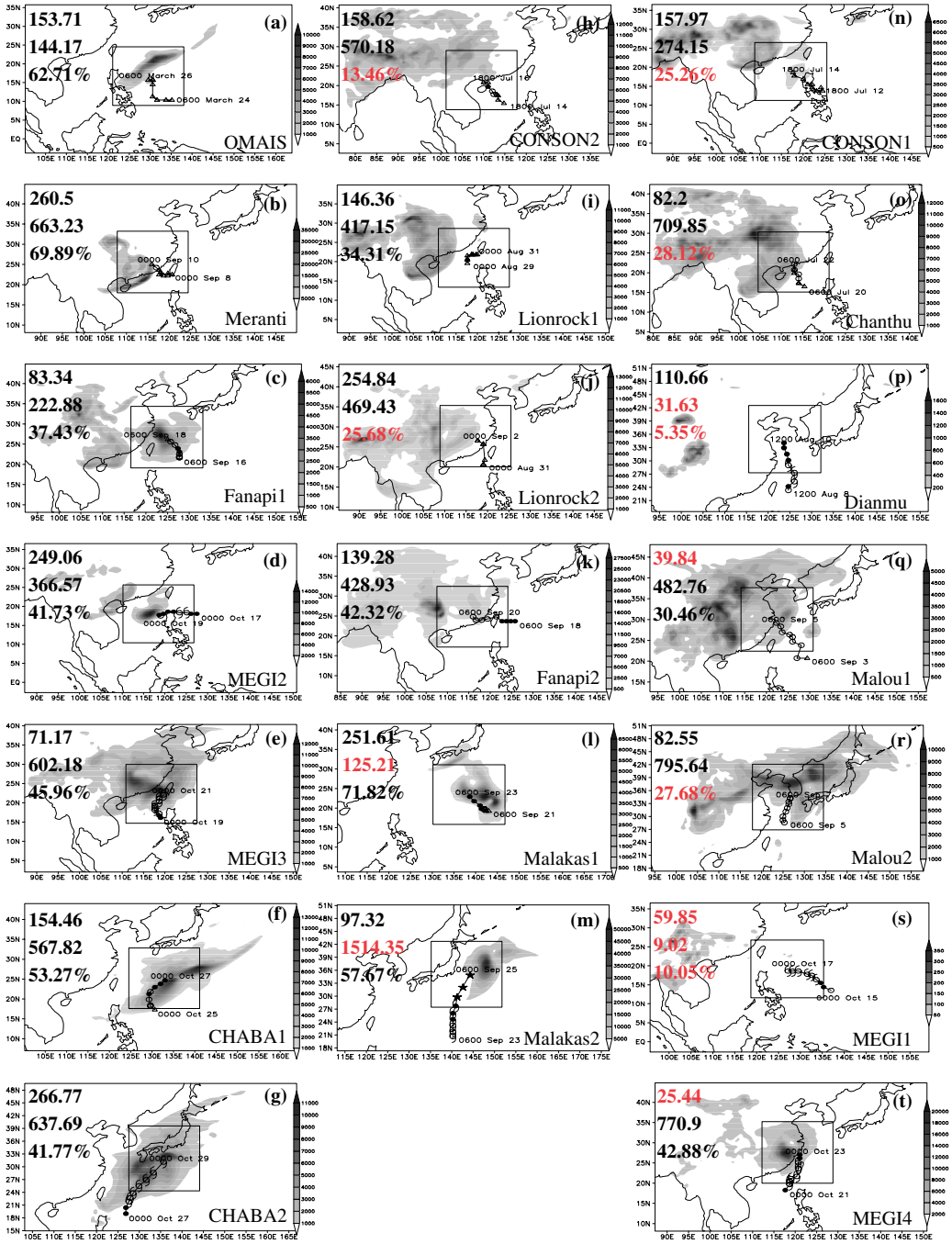

Figure 5. Forecast errors (shaded; J kg^{-1}) for those cases that satisfied all four conditions (a)–(g), those that did not meet all four conditions but showed neutral or moderate track forecast improvements (h)–(m), and those that showed a decline in forecast accuracy (n)–(t). Numbers in the upper left corner of each plot denote the mean track forecast errors (without dropwindsonde data; km) from 12 to 48 h, the scale of the increase in forecast errors between the initial and terminal times, and the proportion of forecast errors within the verification region. Red numbers indicate that the corresponding condition was not satisfied.

conditions were defined that are often required to obtain profound improvements in TC track forecast accuracy from adaptive observations based on CNOP sensitivity.

Of the 20 TC cases, 13 showed neutral or reductions in track forecast errors of between 0% and 51.2% when additional observational data were obtained from the sensitive regions identified by CNOPs. Eliminating initial errors, either those directly related to the storm, or indirectly to the surrounding atmospheric regime at the time, improved the track forecast accuracy. An average relative fall in forecast accuracy was seen in the other 7 cases during the 48 h period. A highly accurate forecast made without dropwindsonde data, the insensitivity of forecast errors to initial errors, or a weak TC regime that could not dominate the main forecast errors over the whole model region led to a decline in forecast accuracy.

Based upon these OSSE results, the following four conditions were defined under which adaptive observations according to CNOP sensitivity have a profound positive impact on TC track forecasts: (i) the track forecast errors associated with forecasts made without dropwindsonde data cannot be ignored; (ii) the forecast errors should be properly sensitive to the initial errors; (iii) the forecast errors in the verification region must account for a large proportion of the total errors from the whole model region; and (iv) the TC should be the dominant regime within the verification

region. Seven TC cases satisfied these four conditions, and showed a 28.75% reduction in the mean track error in the 12–48 h track forecasts.

We expect that the four conditions described above can be applied to TC forecast. It is therefore necessary to discuss their applicability. Since the true TC track cannot be known ahead of time, the first condition is impossible to determine beforehand; nevertheless, we can use the ensemble variance as a surrogate to the track forecast errors. The sensitivity of forecast errors to initial errors shown in the second condition is also a struggle to determine a priori, which should be explored in depth in future work. As indicated in Duan *et al.*(2012), the initial anomalies of the CNOP structure are most likely to evolve into an El Niño event; and such CNOP-induced El Niño events are most sensitive to initial conditions. This result implies that the forecast errors of CNOP-induced El Niño events are significantly sensitive to initial errors (Mu *et al.*, 2007). Along this thinking, we may investigate what initial anomalous states are most likely to cause a TC; then the TC induced by such optimal initial anomalous states could be most sensitive to initial conditions. In TC forecast, we may observe the initial anomalous states in advance to roughly estimate which TC is significantly sensitive to initial conditions. Such study can also help to determine the third and fourth conditions. It seems that the third condition is a necessary consequence of both the first and the fourth conditions, because the verification region is principally defined by the TC vortex, and the position of the TC vortex is poorly forecast. Nevertheless, in some occasions, the TC was the main atmospheric regime in the verification region, while the forecast errors in the verification region did not constitute a large proportion of the total error, such as in the case of Chanthu, CONSON1, and Fanapi1 (Figure 5). That is to say, although the TC regime is the main atmospheric regime within the verification region, it is not strong enough to dominate in the whole model region. There could be much stronger atmospheric regimes outside the verification region which occupy most of the forecast errors. Hence we still classified four conditions to separate the improved from degraded forecasts.

Adaptive observation for TCs is still an unresolved problem, although track forecast has made great improvements these decades. This study reveals the conditions under which CNOP sensitivity is valid for TC-adaptive observations and demonstrates that the TC cases with profound track forecast improvements by using dropwindsondes often have some common characteristics. These results encourage us to perform adaptive observation according to CNOP sensitivity, finally improving the forecast skill of TC track. Despite thus, there are problems, such as how to know a priori which TC case satisfies the four conditions discussed above, still to be explored. Furthermore, we note that the present study only considers the track forecast of TC cases and does not include the intensity forecast. How to improve the intensity forecast of the TCs by adaptive observation may also be a challenging problem. All of these should be further investigated in future in-depth studies. Nevertheless, it is still expected that the results from this study can provide useful information for the TC track forecast.

Acknowledgements

This work was jointly sponsored by the National Science and Technology Support Program (Grant. No. 2012BAC22B03), and the National Nature Scientific Foundations of China (Grant. Nos. 41105040 and 40830955). We thank both the anonymous reviewers for their valuable comments and suggestions.

References

Aberson SD. 2002. Two years of operational hurricane synoptic surveillance. *Weather Forecast.* **17**: 1101–1110.
Aberson SD. 2003. Targeted observations to improve operational tropical cyclone track forecast guidance. *Mon. Weather Rev.* **131**: 1613–1628.
Aberson SD. 2010. 10 years of hurricane synoptic surveillance (1997–2006). *Mon. Weather Rev.* **138**: 1536–1549.
Birgin EG, Martinez JE, Marcos R. 2001. Algorithm 813: SPG – software for convex-constrained optimization. *ACM Trans. Math. Softw.* **27**: 340–349.
Bishop CH, BJ Etherton, SJ Majumdar. 2001. Adaptive sampling with the ensemble transform Kalman filter. Part I: Theoretical aspects. *Mon. Weather Rev.* **129**: 420–436.
Burpee RW, JL Franklin, SJ Lord, RE Tuleya, SD Aberson. 1996. The impact of omega dropwindsondes on operational hurricane track forecast models. *Bull. Am. Meteorol. Soc.* **77**: 925–933.
Chen BY. 2011. Observation system experiments for typhoon Nida (2004) using the CNOP method and DOTSTAR data. *Atmos. Ocean. Sci. Lett.* **4**: 118–123.
Chen BY, Mu M. 2012. The roles of spatial locations and patterns of initial errors in the uncertainties of tropical cyclone forecasts. *Adv. Atmos. Sci.* **29**: 63–78.
Chou KH, Wu CC, Lin PH, Aberson SD, Weissmann M, Harnisch F, Nakazawa T. 2011. The Impact of dropwindsonde observations on typhoon track forecasts in DOTSTAR and T-PARC. *Mon. Weather Rev.* **139**: 1728–1743.
Duan WS, Luo HY. 2010. A new strategy for solving a class of constrained nonlinear optimization problems related to weather and climate predictability. *Adv. Atmos. Sci.* **27**: 741–749.
Duan WS, Mu M, Wang B. 2004. Conditional nonlinear optimal perturbation as the optimal precursors for El Niño–Southern oscillation events. *J. Geophys. Res.* **109**: D23105, DOI: 10.1029/2004JD004756.
Duan WS, Xue F, Mu M. 2009. Investigating a nonlinear characteristic of El Niño events by conditional nonlinear optimal perturbation. *Atmos. Res.* **94**: 10–18.
Duan WS, Yu YS, Xu H, Zhao P. 2012. Behaviors of nonlinearities modulating the El Niño events induced by optimal precursory disturbances. *Clim. Dynam.* DOI: 10.1007/s00382-012-1557-z.
Ehrendorfer M, JJ Tribbia. 1997. Optimal prediction of forecast error covariances through singular vectors. *J. Atmos. Sci.* **54**: 286–313.
Elsberry RL, Harr PA. 2008. Tropical cyclone structure (TCS08) field experiment science basis, observational platforms, and strategy. *Asia–Pacific J. Atmos. Sci.* **44**: 209–231.
Harnisch F, Weissmann M. 2010. Sensitivity of typhoon forecasts to different subsets of targeted dropsonde observations. *Mon. Weather Rev.* **138**: 2664–2680.
Hoffman RN, Grassotti C, Isaacs RG, Louis JF, Nehrkorn T. 1990. Assessment of the impact of simulated satellite lidar wind and retrieved 183 GHz water vapor observations on a global data assimilation system. *Mon. Weather Rev.* **118**: 2513–2542.
Jiang ZN, Wang DH. 2010. A study on precursors to blocking anomalies in climatological flows by using conditional nonlinear optimal perturbations. *Q. J. R. Meteorol. Soc.* **136**: 1170–1180.
Jiang ZN, Wang DH. 2011. Conditional nonlinear optimal perturbations: behaviour during the evolution of cold vortices over northeast China. *Q. J. R. Meteorol. Soc.* **138**: 198–208.
Jiang ZN, Mu M, Wang DH. 2011. Optimal perturbations triggering weather regime transitions: onset of blocking and strong zonal flow. *Adv. Atmos. Sci.* **28**: 59–68.
Langland RH, Toth Z, Gelaro R, Szunyogh I, Shapiro MA, Majumdar SJ, Morss RE, Rohaly GD, Velden C, Bond N, Bishop CH. 1999. The North Pacific Experiment (NORPEX-98): targeted observations for improved North American weather forecasts. *Bull. Am. Meteorol. Soc.* **80**: 1363–1384.
Liu DC, Nocedal J. 1989. On the limited memory BFGS method for large scale optimization. *Math. Program.* **45**: 503–528.

Mu M, Jiang ZN. 2011. Similarities between optimal precursors that trigger the onset of blocking events and optimally growing initial errors in onset prediction. *J. Atmos. Sci.* **68**: 2860–2877.
Mu M, Zhang ZY. 2006. Conditional nonlinear optimal perturbations of a barotropic model. *J. Atmos. Sci.* **63**: 1587–1604.
Mu M, Duan WS, Wang B. 2003. Conditional nonlinear optimal perturbation and its applications. *Nonlinear Proc. Geophys.* **10**: 493–501.
Mu M, Sun L, Hank DA. 2004. The sensitivity and stability of the ocean's thermocline circulation to finite amplitude fresh water perturbations. *J. Phys. Oceanogr.* **34**: 2305–2315.
Mu M, Duan WS, Wang B. 2007. Season-dependent dynamics of nonlinear optimal error growth and ENSO predictability in a theoretical model. *J. Geophys. Res.* **112**: D10113, DOI:10.1029/2005JD006981.
Mu M, Zhou FF, Wang HL. 2009. A method for identifying the sensitive areas in targeted observations for tropical cyclone prediction: conditional nonlinear optimal perturbation. *Mon. Weather Rev.* Special collection: 1623–1639.
Palmer TN, Gelaro R, Barkmeijer J, Buizza R. 1998. singular vectors, metrics, and adaptive observations. *J. Atmos.Sci.* **55**: 633–653.
Powell MJD. 1982. 'VMCWD: A FORTRAN subroutine for constrained optimization'. DAMTP Report 1982/NA4, University of Cambridge, UK.
Qin XH, Mu M. 2011a. A study on the reduction of forecast error variance by three adaptive observation approaches for tropical cyclone prediction. *Mon. Weather Rev.* **139**: 2218–2232.
Qin XH, Mu M. 2011b. Influence of conditional nonlinear optimal perturbations sensitivity on typhoon track forecasts. *Q. J. R. Meteorol. Soc.* **138**: 185–197.
Sun GD, Mu M. 2009. Nonlinear feature of the abrupt transitions between multiple equilibria states of an ecosystem model. *Adv. Atmos. Sci.* **26**: 293–304.
Sun GD, Mu M. 2011. Response of a grassland ecosystem to climate change in a theoretical model. *Adv. Atmos. Sci.* **28**: 1266–1278.
Sun GD, Mu M. 2012. inducing unstable grassland equilibrium states due to nonlinear optimal patterns of initial and parameter perturbations: theoretical models. *Adv. Atmos. Sci.* **29**: 79–90.
Sun GD, Mu M, Zhang YL. 2010. Algorithm studies on how to obtain a conditional nonlinear optimal perturbation (CNOP). *Adv. Atmos. Sci.* **27**: 1311–1321.
Sun L, Mu M, Sun DJ, Yin XY. 2005. Passive mechanism of decadal variation of thermohaline circulation. *J. Geophys. Res.* **110**: C07025, DOI: 10.1029/2005JC002897.
Wang B, Tan XW. 2009. A fast algorithm for solving CNOP and associated target observation tests. *Acta Meteorol. Sin.* **23**: 387–402.
Wang HL, Mu M, Huang XY. 2011. Application of conditional nonlinear optimal perturbations to tropical cyclone adaptive observation using the Weather Research Forecasting (WRF) model. *Tellus* **63A**: 939–957.
Weissmann M, Harnisch F, Wu CC, Lin PH, Ohia Y, Yamashita K, Kim YH, Jeon EH. 2010. The influence of assimilating dropsonde data on typhoon track and mid-latitude forecasts. *Mon. Weather Rev.* **139**: 908–920.
Weissmann M, Langland RH, Cardinali C, Pauley PM, Rahm S. 2012. Influence of airborne Doppler wind lidar profiles near Typhoon Sinlaku on ECMWF and NOGAPS forecasts. *Q. J. R. Meteorol. Soc.* **138**: 118–130.
Wu CC, Lin P-H, Chou K-H, Yeh T-C. 2005. Dropwindsonde observations for typhoon surveillance near the Taiwan region (DOSTAR): an overview. *Bull. Am. Meteorol. Soc.* **86**: 787–790.
Wu CC, Chou KH, Lin PH, Aberson SD, Peng MS, Nakazawa T. 2007. The impact of dropwindsonde data on typhoon track forecasts in DOTSTAR. *Weather Forecast.* **22**: 1157–1176.
Yu YS, Duan WS, Xu H, Mu M. 2009. Dynamics of nonlinear error growth and season-dependent predictability of El Niño events in the Zebiak–Cane model. *Q. J. R. Meteorol. Soc.* **135**: 2146–2160.
Yu YS, Mu M, Duan WS. 2012a. Does model parameter error cause a significant 'spring predictability barrier' for El Niño events in the Zebiak–Cane model? *J. Climate* **25**: 1263–1277.
Yu YS, Mu M, Duan WS, Gong T. 2012b. Contribution of the location and spatial pattern of initial error to uncertainties in El Niño predictions. *J. Geophys. Res.* **117**: C06018, DOI:10.1029/2011JC007758.
Zhou FF, Mu M. 2011. The impact of verification area design on tropical cyclone targeted observations based on the CNOP Method. *Adv. Atmos. Sci.* **28**: 997–1010.
Zhou FF, Mu M. 2012a. The impact of horizontal resolution on the CNOP and on its identified sensitive areas for tropical cyclone predictions. *Adv. Atmos. Sci.* **29**: 36–46.
Zhou FF, Mu M. 2012b. The time and regime dependences of sensitive areas for tropical cyclone prediction using the CNOP method. *Adv. Atmos. Sci.* **29**(4): 705–716.

